**The EMBO Journal (2010) 29,** 1499–1509 | © 2010 European Molecular Biology Organization | All Rights Reserved 0261-4189/10
www.embojournal.org

THE EMBO JOURNAL

# USP9x-mediated deubiquitination of EFA6 regulates *de novo* tight junction assembly

**Delphine Théard[1], Florian Labarrade[1], Mariagrazia Partisani[1], Julie Milanini[1], Hiroyuki Sakagami[2], Edward A Fon[3], Stephen A Wood[4], Michel Franco[1] and Frédéric Luton[1,*]**

[1]CNRS UMR6097, Institut de Pharmacologie Moléculaire et Cellulaire, Université de Nice Sophia-Antipolis, Valbonne, France, [2]Department of Anatomy, Kitasato University School of Medicine, Kitasato, Japan, [3]Montreal Neurological Institute, McGill University, Montréal, Québec, Canada and [4]National Centre for Adult Stem Cell Research, Griffith University, Nathan, Queensland, Australia

**In epithelial cells, the tight junction (TJ) functions as a permeability barrier and is involved in cellular differentiation and proliferation. Although many TJ proteins have been characterized, little is known about the sequence of events and temporal regulation of TJ assembly in response to adhesion cues. We report here that the deubiquitinating enzyme USP9x has a critical function in TJ biogenesis by controlling the levels of the exchange factor for Arf6 (EFA6), a protein shown to facilitate TJ formation, during a narrow temporal window preceding the establishment of cell polarity. At steady state, EFA6 is constitutively ubiquitinated and turned over by the proteasome. However, at newly forming contacts, USP9x-mediated deubiquitination protects EFA6 from proteasomal degradation, leading to a transient increase in EFA6 levels. Consistent with this model, USP9x and EFA6 transiently co-localize at primordial epithelial junctions. Furthermore, knockdown of either EFA6 or USP9x impairs TJ biogenesis and EFA6 overexpression rescues TJ biogenesis in USP9x-knockdown cells. As the loss of cell polarity is a critical event in the metastatic spread of cancer, these findings may help to understand the pathology of human carcinomas.**
*The EMBO Journal* (2010) **29,** 1499–1509. doi:10.1038/emboj.2010.46; Published online 25 March 2010
*Subject Categories*: cell & tissue architecture; proteins
*Keywords*: EFA6; proteasome; tight junction; USP9x

## Introduction

Polarized epithelial cells are adjoined through intercellular junctions arranged along their lateral membrane domains. In general, adhesion is provided by the adherens junction (AJ), mediated by homotypic calcium-dependent interactions between transmembrane E-cadherin molecules. The tight junction (TJ) is located at the most apical point of the lateral membrane, where it functions as a permeability barrier and is involved in various functions including cellular differentiation and proliferation (Tsukita *et al*, 2001, 2008). Both, AJ and TJ are associated with the actin cytoskeleton through cytosolic proteins that bridge the cytoplasmic tail of the junctional transmembrane proteins with the actin filaments. A model of TJ biogenesis during epithelial polarization is emerging whereby cell–cell contacts are initially engaged by nectin and E-cadherin. At these newly formed contact zones, the underlying actin is rearranged to stabilize and strengthen the cell–cell adhesion. TJ proteins are then recruited to the sites of cadherin-mediated cell–cell contacts and eventually segregate away from the contact zone to form a distinct junctional complex bound to a dense circumferential ring of acto-myosin (Drubin and Nelson, 1996; Miyoshi and Takai, 2005). During this process, the polarity complexes Crumbs/Pals/PATJ and Scribble/Lgl function to determine the apico-basal polarity, whereas the Par3/Par6/aPKC complex is believed to define the landmark where the TJ will form (Shin *et al*, 2006; Goldstein and Macara, 2007). Despite the intense effort to characterize the composition and organization of TJs at the molecular level, the temporal regulation of TJ biogenesis in response to *de novo* E-cadherin-mediated cell–cell adhesion remains poorly understood.

The EFA6 family is composed of four members EFA6A, B, C and D, each encoded for by a different gene. Additional isoforms generated by alternative splicing have been described for EFA6A (Sironi *et al*, 2009), and possibly EFA6B (Derrien *et al*, 2002; Luton *et al*, 2004; Supplementary Figure S1A and B) and EFA6C (Matsuya *et al*, 2005). The tissue distribution has been mostly studied at the mRNA level in the mouse brain. Three EFA6 members (EFA6A, EFA6C and EFA6D) are abundantly expressed in the brain where they display overlapping but distinct expression patterns (Sakagami, 2008). EFA6C seems to be restricted to neuronal tissues (Derrien *et al*, 2002; Matsuya *et al*, 2005), whereas a small EFA6A RNA messenger was also found in the small intestin and colon (Derrien *et al*, 2002; Sironi *et al*, 2009). EFA6D mRNA is ubiquitously expressed with the highest levels in liver, lung and thymus (Sakagami *et al*, 2006). EFA6B mRNA was found widely expressed in epithelial tissues (Derrien *et al*, 2002). In addition, anti-EFA6B immunoblots reveal the presence of a 66 kDa protein in most tissues specially in the kidney, and a protein of 175 kDa with high expression in the thymus, spleen and lungs (Derrien *et al*, 2002; Supplementary Figure S1A and B). All EFA6 proteins follow a general structure that is comprised of a divergent N-terminal domain, the conserved catalytic Sec7 domain, a PH domain responsible for membrane localization and a C-terminal region involved in the rearrangement of the actin cytoskeleton (Franco *et al*, 1999; Derrien *et al*, 2002; Luton *et al*, 2004; Klein *et al*, 2008). The best-characterized isoforms, EFA6A and EFA6B, have been found to function similarly regarding their ability to catalyse Arf6 nucleotide exchange activity, their subcellular distribution and their effects

*Corresponding author. CNRS UNSA UMR6097, Institut de Pharmacologie Moléculaire et Cellulaire, 660 Route des Lucioles, Valbonne 6560, France. Tel.: + 33 04 93 95 77 70; Fax: + 33 04 93 95 77 08; E-mail: luton@ipmc.cnrs.fr

**Received: 15 February 2010; accepted: 3 March 2010; published online: 25 March 2010**

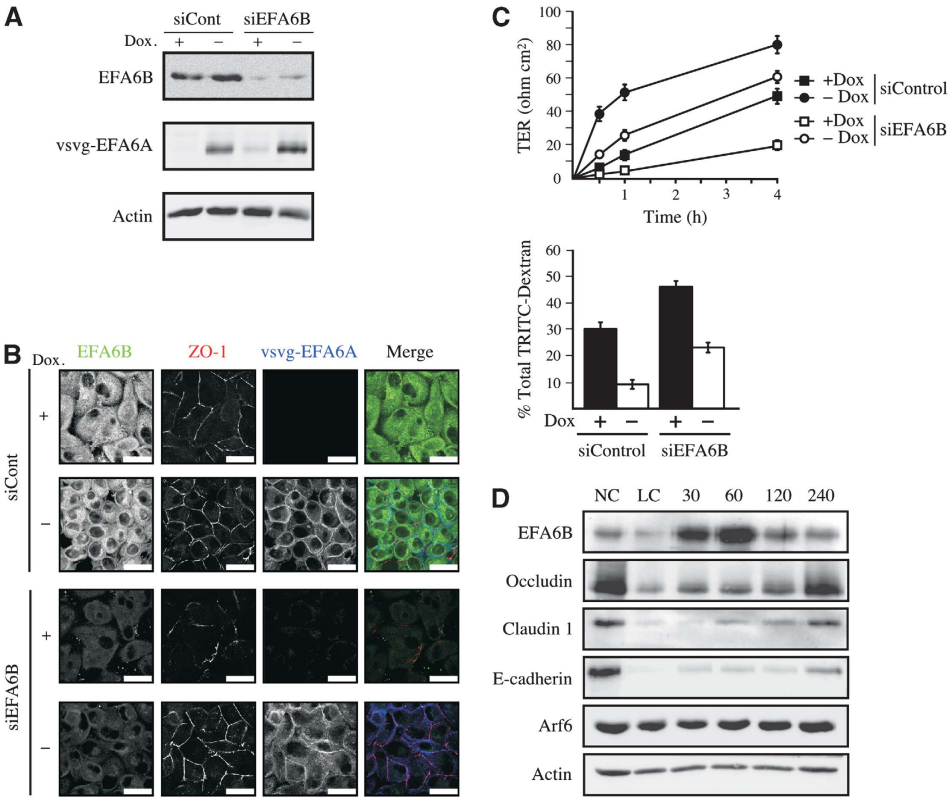


**Figure 1** EFA6B is required for efficient TJ assembly. (**A**) Immunoblot showing EFA6B, vsvg-EFA6A and actin levels in tet-off regulated vsvg-EFA6A MDCK cells grown in the absence or presence of doxycyclin (−/+Dox) and transiently transfected with control or EFA6B-specific siRNA #637. (**B**) The indicated cells were subjected to a calcium switch, fixed 90 min after calcium repletion, and processed for immunofluorescence analysis. The expression and localization of EFA6B (green), ZO-1 (red) and vsvg-EFA6A (blue) were examined. Scale bars, 25 μm. (**C**) The gain of TJ barrier function was analysed in a calcium switch assay by measuring the TER over time and the paracellular diffusion of TRITC-dextran at 2 h after calcium repletion +/−siEFA6B #637. For TER measurement $n=5$ and error bars represent the s.e.m. For siControl cells +/−Dox $P<0.001$ at all times, for siEFA6B cells +/−Dox $P<0.002$ at all times, for +Dox cells +/−siEFA6B $P<0.005$ after 30 min, for −Dox cells +/−siEFA6B $P<0.01$ at all times. For the paracellular diffusion of the TRITC-dextran $n=3$ and error bars represent s.e.m. For siControl cells +/−Dox $P=0.0017$, for siEFA6B cells +/−Dox $P=0.0011$, for +Dox cells +/−siEFA6B $P=0.0073$, for −Dox cells +/−siEFA6B $P=0.0066$. (**D**) The expression of EFA6B, occludin, claudin 1, E-cadherin, Arf6 and actin was analysed by immunoblotting during a calcium switch assay at the indicated times (min) after calcium repletion. NC, cells kept in normal calcium medium; LC, cells incubated 4 h in low calcium medium and lysed before calcium repletion.

on the actin cytoskeleton organization. Further, the PH-Cter constructs of EFA6A and EFA6B both localize and affect the actin cytoskeleton organization similarly (Derrien *et al*, 2002; Luton *et al*, 2004; Klein *et al*, 2008; unpublished data).

Previously, we have shown that overexpression of EFA6A accelerated the formation of the TJ by contributing to the reorganization of the apical actin cytoskeleton in Madin-Darby canine kidney (MDCK) cells (Luton *et al*, 2004). Our current results show that endogenous EFA6B is required for efficient TJ biogenesis. Protein levels of EFA6B increase both temporally and spacially just at the point of cell–cell contact. In addition, we report here that EFA6B is constitutively degraded by the proteosome machinary, and that USP9x-mediated deubiquitination is responsible for the build-up of EFA6B levels during the establishment of cell polarity. USP9x has been found to translocate transiently to primordial cell–cell contacts, thereby ensuring the proper spatiotemporal activity of EFA6B, and thus, coordinating the timing of TJ assembly.

## Results

To further investigate the function of EFA6 during TJ biogenesis, we used small interfering RNA (siRNA) to reduce endogenous EFA6B levels in MDCK cells (Supplementary Figure S1C). As a control, the human vsvg-EFA6A, which is insensitive to the canine EFA6B siRNA, was expressed in EFA6B-knockdown cells (Figure 1A). EFA6B-knockdown cells were much slower at forming TJ with only a few cells displaying a partial ZO-1 staining at their periphery (Figure 1B). The delay in TJ assembly was completely rescued by vsvg-EFA6A overexpression. EFA6B knockdown did not affect the expression of Arf6 or of the constitutive TJ or AJ proteins (Supplementary Figure S1C). Cells overexpressing vsvg-EFA6A assembled their TJ at a faster rate than control cells with a majority (≈60% of the cells) being totally surrounded by ZO-1 staining compared with <20% for the control cells. At the level of TJ function, EFA6B knockdown increased the diffusion of TRITC-dextran and delayed the acquisition of transepithelial resistance (TER), whereas vsvg-EFA6A overexpression reduced TRITC-dextran diffusion and accelerated the gain of TER (Figure 1C). Importantly, the effects of EFA6B knockdown on TRITC-dextran diffusion and TER acquisition could be rescued by overexpressing wild type, but not by mutants of EFA6A that are either catalytically inactive (vsvg-EFA6A-E242K) or defective in actin remodelling (vsvg-EFA6A-ΔCter) (Supplementary Figure S2A). Thus,

both the GEF activity in the Sec7 domain and a non-catalytic actin remodelling activity in the C-terminal domain are required for EFA6 to efficiently orchestrate TJ assembly. Next, we examined endogenous EFA6B levels in MDCK cells that were induced to polarize by a calcium switch procedure. We found that EFA6B levels increased 30 min after calcium repletion (Figure 1D). EFA6B protein levels reached a peak of $8.7 \pm 0.8$ fold increase compared with cells grown in normal calcium ($n = 9$) at 60–90 min, and returned to baseline after 4–6 h. In contrast, the levels of Arf6 did not vary significantly. As previously shown, occludin, claudin 1 and E-cadherin levels decreased rapidly after calcium withdrawal and slowly recovered upon calcium repletion. Importantly, EFA6B accumulation did not coincide with changes in other TJ proteins and occurred before the appearance of the high molecular weight phosphorylated forms of occludin, which is associated with its incorporation into TJs (Sakakibara *et al*, 1997; Wong, 1997).

Considering the dramatic variations in EFA6B levels during the induction of cell polarity, we asked whether EFA6B levels could be under the control of the ubiquitin-proteasome system, the main pathway for degradation of cytosolic proteins (Hershko and Ciechanover, 1998). In both non-polarized (Figure 2A) and fully polarized (data not shown) MDCK cells, EFA6B accumulation correlates with the concentration and duration of exposure to the proteasome inhibitors lactacystin and MG-132. These results suggest that, at steady state, EFA6B is rapidly turned over by the proteasome. Indeed, EFA6B displays a short half-life and a rapid rate of protein synthesis that can account for the rapid modulation of EFA6B levels during cell polarization (Supplementary Figure S2B). Next, we analysed whether EFA6B was ubiquitinated in MG-132 treated MDCK cells. The anti-ubiquitin antibody P4G7 revealed a major band at $\approx$97 kDa corresponding to EFA6B (66 kDa) attached with four molecules of ubiquitin (Figure 2B, left panel). When the same samples were analysed with the FK1 antibody that recognizes only poly-ubiquitin chains (Figure 2B, right panel), we observed the same major band at $\approx$97 kDa demonstrating that EFA6B is not multi-monoubiquitinated but rather poly-ubiquitinated. The poly-ubiquitination status was confirmed in pull-down experiments using the ubiquitin-binding domain of the proteasome subunit S5a that recognizes poly-ubiquitin compared with the very weak signal using the domain of Eps15 that preferentially bind mono-ubiquitin (Woelk *et al*, 2006) (Supplementary Figure S2C). Thus, EFA6B is constitutively poly-ubiquitinated and degraded by the proteasome. Next, we asked whether endogenous EFA6B was poly-ubiquitinated during epithelial cell polarization. In the absence of proteasome inhibitors, filter-grown MDCK cells were subjected to a calcium switch and the EFA6B immunoprecipitated at different times after calcium repletion. The anti-poly-ubiquitin antibody revealed a major band at $\approx$97 kDa and some much higher molecular weigh bands appearing at about 60 min after calcium repletion (Figure 2C, left panel). After stripping, the membrane was re-probed with the anti-EFA6B antibody to ascertain whether those bands were poly-ubiquitinated forms of EFA6B (Figure 2C, right panel). The unmodified EFA6B migrates at 66 kDa, indicating that the $\approx$97 kDa band corresponds to the addition of a chain of four ubiquitin molecules. An extra band at about 105 kDa corresponding to the addition of five ubiquitin molecules is also detected

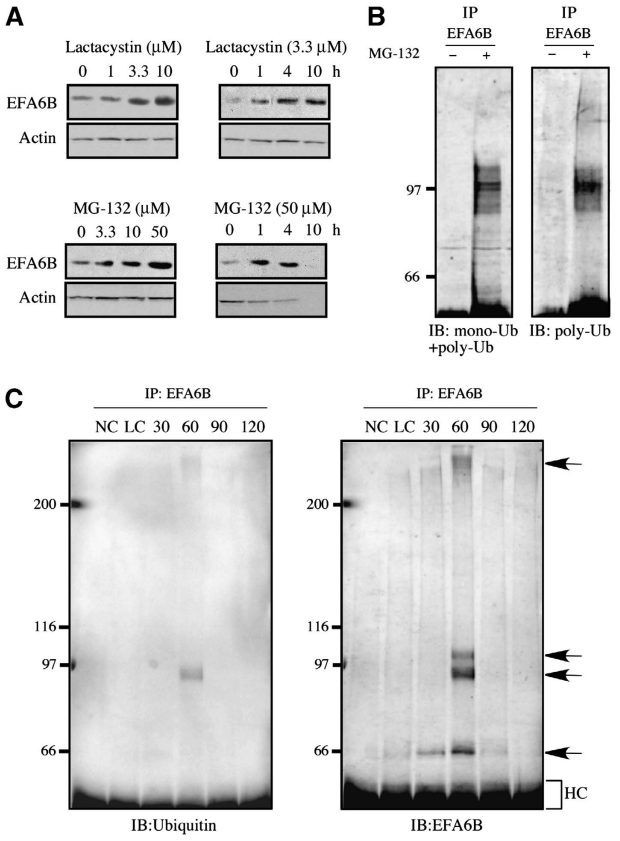


**Figure 2** EFA6B is a substrate of the ubiquitin-proteasome system. (**A**) MDCK cells were grown in the presence of lactacystin or MG-132 and lysed at the indicated times. The lysates were resolved by SDS–PAGE and immunoblotted to determine the amount of EFA6B and, as a loading control, actin. The left panels show a dose response to increasing amounts of the indicated drugs for 2 h and the right panels show a time course for the indicated concentration of the drugs. Cells toxicity to 50 μM MG-132 at 10 h explains the weak signal. (**B**) MDCK cells were treated or not with MG-132 (50 μM) for 4 h and endogenous EFA6B (66 kDa) immunoprecipitated. The two samples were deposited twice side-by-side on a poly-acrylamide gel and resolved by electrophoresis. After transfer, the immunoblots were probed separately either with the anti mono- and poly-ubiquitin antibody (P4G7) or the anti poly-ubiquitin antibody (FK1). (**C**) MDCK cells grown on filters in the absence of proteasome inhibitors were subjected to a calcium switch and incubated after calcium repletion for the indicated times. NC, normal calcium medium; LC, low calcium medium. After lysis, the samples were resolved on SDS–PAGE, immunoblotted and probed first with the anti poly-ubiquitin (FK1) antibody. After stripping, the membrane was then probed with the anti-EFA6B antibody. The arrows point to the non-ubiquitinated (66 kDa) and poly-ubiquitinated EFA6B. HC, heavy chain from the immunoprecipitating antibody.

though barely visible in the anti-ubiquitin immunoblot. In our calcium switch experiments, we have always observed a strong and robust poly-ubiquitination of EFA6B with high molecular weight moieties. However, we have never detected poly-ubiquitinated forms smaller than $\approx$97 kDa, suggesting that a minimal chain of four ubiquitin molecules is added at once. Typically, the poly-ubiquitination of EFA6B was only seen during a very narrow time window, suggesting that it is subsequently degraded very rapidly. At the peak of ubiquitination, $53.3 \pm 17.5\%$ ($n = 8$) of the total EFA6B was poly-ubiquitinated, which is considerable considering that the cells were not transfected with ubiquitin nor treated with proteasome inhibitors. Together, our data identify a pool of

EFA6B, which after accumulating during the initial stages of epithelial polarization is rapidly poly-ubiquitinated and degraded by the proteasome.

We reasoned that a straightforward mechanism to account for the rapid increase in EFA6B levels would be through protection from the proteasome by deubiquitination. Thus, we looked for a DUB that would act on EFA6B upon E-cadherin engagement. USP9x is a DUB that has been reported to affect two junctional proteins, β-catenin and afadin, and to associate with E-cadherin in subconfluent epithelial cells, raising the possibility that USP9x might be a key DUB in cell polarization (Taya *et al*, 1998, 1999; Murray *et al*, 2004). We set out to observe an interaction between endogenous USP9x and EFA6B through co-precipitation. To co-precipitate USP9x and EFA6B from MDCK cells, we performed a calcium switch and lysed the cells at various times after calcium repletion. USP9x could be co-precipitated together with EFA6B only at 45 min after calcium repletion, indicating that the interaction between endogenous EFA6B and USP9x is transient and occurs predominantly at early time points during cell–cell adhesion (Figure 3A). Next, we performed pull-down experiments using four fragments of USP9x, encompassing the entire molecule, fused to GST. Only the fragment N2 (674–1218) could bind directly to purified his-EFA6A (Figure 3B). We also performed pull-down experiments using several fragments of EFA6A fused to GST (Figure 3C). Endogenous USP9x from MDCK lysate was pulled down with GST-EFA6A full length, the GST-PHCter, and the GST-PH fragments, but not with GST-Sec7, GST-Cter or GST alone. Thus, the PH domain alone is efficient enough to bind USP9x, and can be used in the cell as a dominant negative for USP9x activity. When used as a dominant negative in MDCK cells, it dramatically slowed down the TJ formation compared with untransfected MDCK cells, whereas consistent with earlier findings, GFP-EFA6A stimulated the TJ formation (Figure 3D; Supplementary Figure S3A). This result suggests that EFA6 binding to USP9x has a function in TJ assembly. Thus, we tested whether USP9x could promote EFA6 deubiquitination in baby hamster kidney (BHK) cells. Expression of V5-USP9x, but not the catalytic point mutant V5-USP9x C1566S, decreased vsvg-EFA6A ubiquitination and increased its levels in BHK cells (Figure 3E).

These results indicate that USP9x deubiquitinates EFA6 in cells, thereby protecting it from degradation by the proteasome. To further explore the function of USP9x, we analysed the effects of siRNA-mediated knockdown of USP9x (Supplementary Figure S3B) on EFA6B, AJ and TJ protein levels. In MDCK USP9x-knockdown cells, afadin expression was dramatically decreased, indicating that it is a constitutive substrate of USP9x (Figure 4A). However, the protein levels of neither EFA6B nor any of the other AJ or TJ proteins were affected by the USP9x knockdown. Nevertheless, the kinetics of EFA6B accumulation suggested that USP9x might only affect EFA6B levels during the early stages of cell polarization. Indeed, over the course of a calcium switch experiment and in the absence of proteasome inhibitors, no accumulation or poly-ubiquitination of EFA6B could be detected in USP9x-knockdown cells (Figure 4B). In contrast, in USP7-knockdown cells, used as a control, EFA6B accumulation and poly-ubiquitination occurred similarly to control MDCK cells (Figures 2D and 4B). These results support our model whereby USP9x is responsible for the transient accumulation of EFA6 protein, and that the observed poly-ubiquitination is due to the release of a synchronized pool of EFA6B no longer under the protective effect of USP9x. It also excluded the possibility that EFA6B accumulation was solely due to an arrest of its poly-ubiquitination. Note that the levels of USP9x remained unchanged during the calcium switch-induced cell–cell contact formation in control USP7-knockdown cells. In addition, except for afadin levels, which were reduced throughout the polarization time course in USP9x-knockdown cells, we never observed changes in the levels of any of the other AJ or TJ components (Supplementary Figure S3C). These results indicate that subsequent to E-cadherin engagement USP9x activity results in EFA6B accumulation.

Next, we compared the subcellular localization of EFA6 and USP9x during the formation of cell–cell contacts. Adjacent cells contact through membrane protrusions such as lamellipodia or filopodia. At the initial stage of cell–cell contacts, which yield to the formation of AJ, primordial spot-like junctions first form at the periphery or tips of these cellular protrusions. E-cadherin and filamentous actin concentrate into these newly formed adhesion points that extend and fuse followed by the recruitment and accumulation of the components of the TJ (Adams *et al*, 1998; Vasioukhin and Fuchs, 2001; Miyoshi and Takai, 2005). Our results show that in non-contacting cells, vsvg-EFA6A was detected at the periphery of lamellipodia and at the tip of filopodia (Figure 5A–A''). When we followed in real-time GFP-EFA6A localization in comparison to E-cadherin-RFP, we detected E-cadherin-RFP at the primordial contacts followed rapidly by co-localization of GFP-EFA6A, typically within 5 min (Figure 5B; full movie Supplementary Figure S4M). As the contact matures, large E-cadherin plaques gradually emerge at the margins (Adams *et al*, 1998) where the GFP-EFA6A signal is increasing and remains tightly co-localized with E-cadherin-RFP (Figure 5C; full movie Supplementary Figure S4N). This increase in the GFP-EFA6A signal at primordial contact supports our biochemical observations where we describe the accumulation of EFA6 (Figure 1; Luton *et al*, 2004). It is interesting to note that the maturation of the contact is coordinated with and dependent on the reorganization of the underlying actin cytoskeleton, and that in several model systems, EFA6 has been shown to affect cytoskeletal organization, which includes the apical actin ring of the TJ (Franco *et al*, 1999; Derrien *et al*, 2002; Luton *et al*, 2004). In mature contacts, vsvg-EFA6A is no longer enriched (Figure 5A''). Subsequently, we investigated the localization of endogenous USP9x using a rabbit polyclonal antibody (Supplementary Figure S4A–G) as GFP-USP9x could not be expressed. USP9x was mostly cytosolic as reported earlier in other cell types (Murray *et al*, 2004; Jolly *et al*, 2009). Yet, similarly to vsvg-EFA6A, a significant fraction was detected at the periphery of lamellipodia and at the tip of filopodia (Figure 5D–D''), where both proteins co-localize (Supplementary Figure S4H). However, in mature contacts of confluent cells, USP9x was totally excluded (Figure 5D''; Supplementary Figure S4K). In contrast, GFP-EFA6A remained visible, although no longer enriched, at more mature contacts (Figure 5A''; Supplementary Figure S4J; Luton *et al*, 2004). More importantly, a careful analysis of newly formed contacts, defined by a short contact zone at the extremity of a membrane protrusion, showed that similarly to GFP-EFA6A, USP9x was concentrated at the primordial junction

 

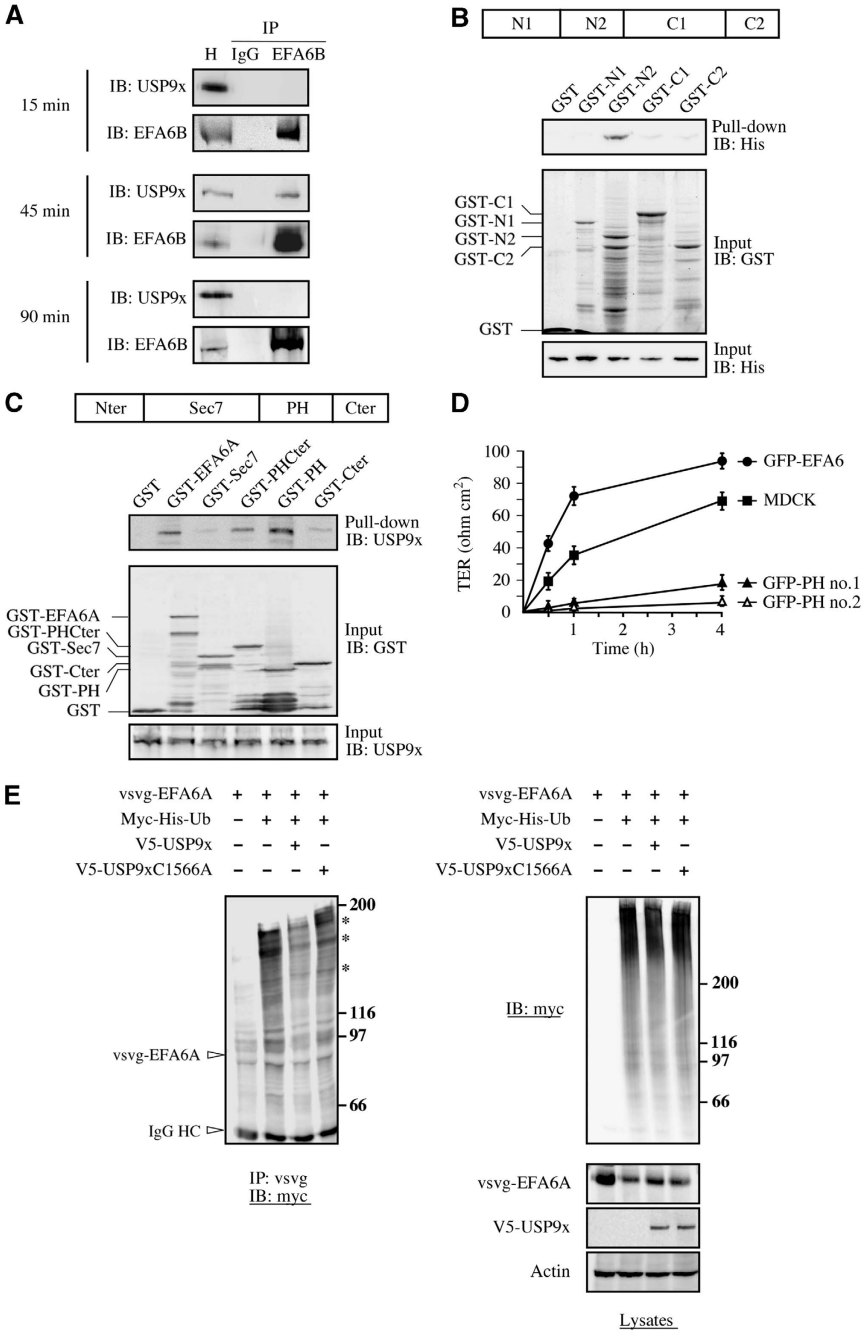


**Figure 3** EFA6 binds directly to and is a substrate of the DUB USP9x (**A**) EFA6B co-immunoprecipitates with USP9x. MDCK cells grown on 24-mm filters and submitted to a calcium switch were solubilized in NP-40 lysis buffer at the indicated times after calcium repletion. The cleared lysates were subjected to immunoprecipitation (IP) with a whole IgG fraction as a negative control or with the anti-EFA6B antibody. After electrophoresis and transfer, the immunoblots (IB) were probed separately with an anti-USP9x antibody and an anti-EFA6B antibody. H, fraction (1/20) of the homogenate used in the IP. (**B**) The N2 (674–1218) domain of USP9x is required for EFA6A direct binding. Schematic representation of the different domains of USP9x fused to GST: N1 (1–674), N2 (674–1218), C1 (1216–2107), C2 (2102–2560). Purified his-EFA6A was incubated for 2 h at 4°C with the indicated GST fusion proteins followed by precipitation with glutathione beads. The precipitates were resolved by SDS–PAGE and the membrane probed with the anti-histidine antibody (upper panel). The middle and lower panels show anti-GST and anti-histidine immunoblots to control for the amount of GST fusion protein and his-EFA6A present in the assay, respectively. (**C**) The PH domain of EFA6A is required for USP9x binding. Schematic representation of the different domains of EFA6A fused to GST used in the pull-down assay. An MDCK cell lysate was incubated for 4 h at 4°C with the indicated GST fusion proteins and precipitated with glutathione beads. The precipitates were resolved by SDS–PAGE and the membrane probed with the anti-USP9x antibody (upper panel). The middle and lower panels show an anti-GST and anti-USP9x immunoblots to control for the amount of GST fusion protein and USP9x present in the assay, respectively. (**D**) The gain of TJ barrier function was analysed in a calcium switch assay by measuring the TER over time. Two MDCK cell lines expressing the PH domain of EFA6A fused to GFP were analysed (GFP-PH #1 and GFP-PH #2) and compared with control or MDCK cells expressing GFP-EFA6A full length. $n = 3$ and error bars represent the s.e.m. For both GFP-PH cell lines and GFP-EFA6A versus MDCK control, $P < 0.05$ at all times. (**E**) USP9x promotes EFA6A deubiquitination in cells. BHK cells were transfected with the indicated constructs. At 24 h post-transfection, the cells were lysed in SDS and vsvg-EFA6A immunoprecipitated with an anti-vsvg antibody. The immunoprecipitates were resolved by SDS–PAGE and the membrane probed with an anti-myc antibody to detect ubiquitinated vsvg-EFA6A. The corresponding lysates were analysed by immunoblotting for their ubiquitination pattern and the expression of vsvg-EFA6A, V5-USP9x and actin. In the immunoprecipitation gel, the non-ubiquitinated vsvg-EFA6A is not visible, but its known position is indicated with an arrow, and the IgG HC arrow points to the heavy chain from the anti-vsvg immunoprecipitating antibody. The asterisks point to the major high molecular weigh bands of the ubiquitinated vsvg-EFA6.

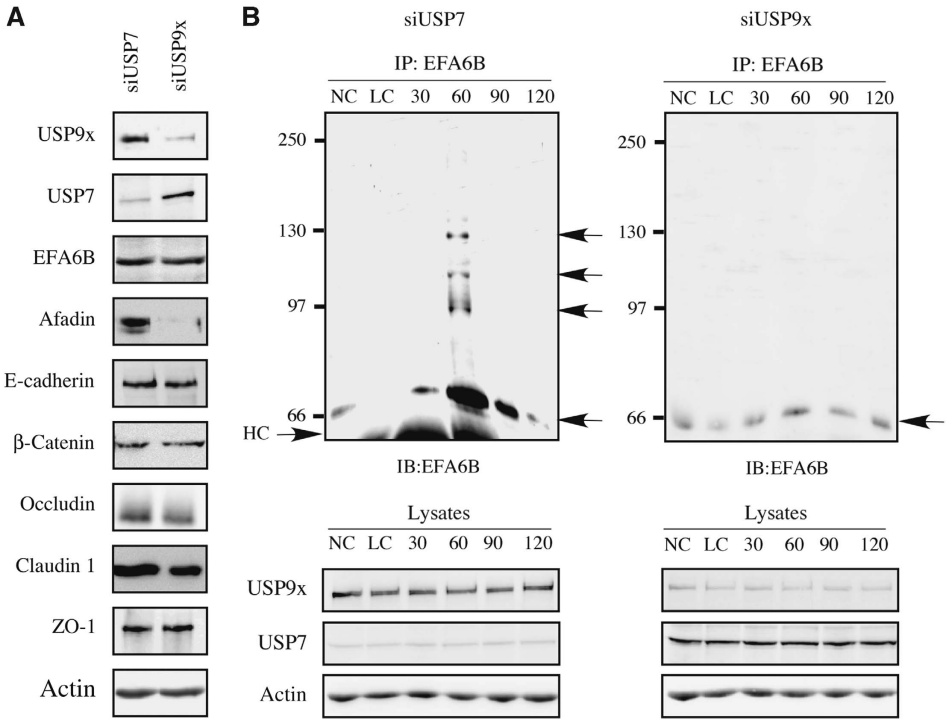


**Figure 4** USP9x controls EFA6B levels and poly-ubiquitination in polarizing MDCK cells. (**A**) Lysates from non-polarized MDCK cells transfected with siRNA directed against USP7 (siRNA #1118) or USP9x (siRNA #182) were resolved by SDS–PAGE and the levels of the indicated proteins analysed by immunoblotting. The same results were obtained with fully polarized cells (data not shown). (**B**) MDCK cells, depleted for USP7 (as a control) or USP9x by RNA interference, were subjected to a calcium switch to induce polarization in the absence of proteasome inhibitors. At the indicated times, endogenous EFA6B was immunoprecipitated. The immunoprecipitates were resolved on SDS–PAGE, and after transfer, the membrane was probed with an anti-EFA6B antibody. The arrows point to the non-ubiquitinated (66 kDa) and poly-ubiquitinated EFA6B of higher molecular weights. A fraction (1/40) of the corresponding lysates at each time point was analysed by immunoblot for the expression of USP7, USP9x and actin. The expression of afadin, β-catenin, E-cadherin, occludin and claudin 1 is shown in Supplementary Figure S3C.

(Supplementary Figure S4L). To enhance detection of primordial junctions, we have submitted MDCK cells expressing GFP-EFA6A to a calcium switch. At 30 min after calcium repletion, many newly formed contacts labelled for E-cadherin could be observed. These primordial junctions were also enriched in both GFP-EFA6A and endogenous USP9x (Figure 5E–G). At calcium repletion times greater than 1 h, USP9x was no longer readily detected at the maturing cell–cell contacts. These findings, together with our biochemical studies, show that EFA6 accumulates at the contact zone and that its levels are temporally and spatially controlled by the DUB activity of USP9x in response to E-cadherin engagement.

Our current model, placing USP9x at the contact zone and acting directly on EFA6, which in turn stabilizes the actin cytoskeleton at the TJ, predicts that depletion of USP9x should have a direct effect on TJ assembly. To test this, a calcium switch was performed on USP9x-knockdown cells and the formation of the TJ was analysed by immunofluorescence. In control cells, the assembly of the TJ, labelled with ZO-1, could be observed 1 h after calcium repletion and was almost complete by 3 h. In contrast, in USP9x-knockdown cells, the TJ was only weakly visible 1 h after calcium addition and did not progress much further by 3 h (Figure 6A). Thus, USP9x and its binding to EFA6B (Figure 3D; Supplementary Figure S3A) are crucial for the assembly of TJs. Furthermore, to determine whether EFA6 is a key substrate of USP9x required for cell polarization, vsvg-EFA6A was expressed in USP9x-knockdown cells (Figure 6B). In these cells, the TJ formed faster than in USP9x-knockdown cells although not as fast as in control cells (Figure 6C). We also measured the gain of TER and the paracellular diffusion of TRITC-dextran (Figure 6D). In USP9x-knockdown cells, both functions were impaired when compared with control cells, and dramatically impaired when compared with control cells overexpressing vsvg-EFA6A. However, both functions could be partially rescued by the expression of vsvg-EFA6A in USP9x-knockdown cells, indicating that EFA6 is a key substrate of USP9x in the early stages of epithelial polarization. The rescue of USP9x-depleted cells by vsvg-EFA6A could be explained by the protection of a pool of vsvg-EFA6A from proteasomal degradation at the site of TJ formation. Other substrates of USP9x may be also necessary at early time points such as afadin. However, exogenous expression of afadin alone or together with vsvg-EFA6A did not rescue the effects of USP9x deficiency on TJ biogenesis (data not shown).

## Discussion

We have uncovered a new regulatory pathway for epithelial cell polarization and TJ formation downstream of cell–cell contacts mediated by E-cadherin. This pathway involves EFA6, the exchange factor for Arf6, and its precise spatio-temporal regulation by the deubiquitinase USP9x. Our current findings map out three important facts. First, protein levels of EFA6B are important to the rate at which the TJ is formed. Second, protein levels of EFA6B are maintained at

 

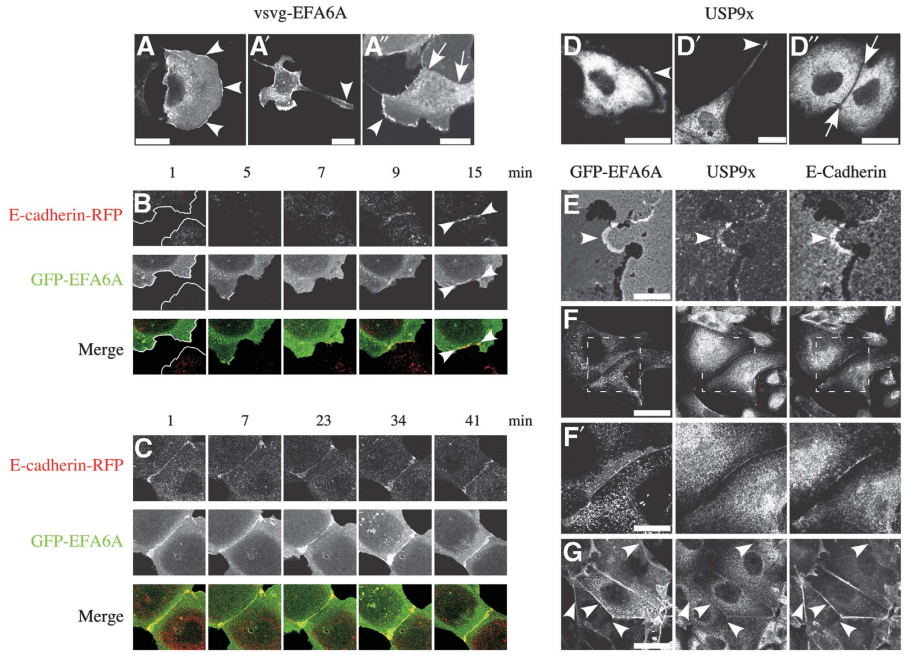


**Figure 5** EFA6B and USP9x transiently co-localize at plasma membrane domains involved in initial cell–cell contact formation in MDCK cells. (**A–A''**) The three panels show the subcellular localization of vsvg-EFA6A in isolated or contacting MDCK cells. The arrowheads point to the enrichment of vsvg-EFA6A at the periphery of membrane ruffles or at the extremity of a long membrane extension. Vsvg-EFA6A is present but no longer concentrated at the contact zone, indicated by arrows, between two adhesive cells (**A''**). (**B**) Images extracted from a movie of two isolated cells establishing a new contact and transfected for the expression of GFP-EFA6A and E-cadherin-RFP. In the first image, the outlines of the non-contacting cells are marked. E-cadherin and EFA6A co-accumulate at the contact zone. The arrows in the last panel point to the newly formed contact co-stained for E-cadherin and EFA6A. (**C**) Images extracted from a movie showing the maturation of a recent contact established between two cells transfected for the expression of GFP-EFA6A and E-cadherin-RFP. It shows that EFA6A accumulates together with E-cadherin at the contact zone as the newly formed contact is maturing. The full movies presented in (**B**, **C**) are shown in Supplementary Figure S4M and N. (**D–D''**) These three panels show the subcellular localization of endogenous USP9x, detected with the N1 antibody (Supplementary Figure S1B) in isolated or contacting MDCK cells. Similar to EFA6, the arrowheads point to the presence of USP9x at the periphery of membrane ruffles (**D**), or at the extremity of a long membrane extension (**D'**). However, unlike EFA6, USP9x is excluded from cell–cell contacts delimited by the arrows (**D''**). (**E–G**) EFA6 and USP9x co-localize transiently at newly formed contacts. GFP-EFA6A MDCK cells submitted to a calcium switch were fixed 30 min after calcium repletion and co-stained for the endogenous USP9x and E-cadherin molecules. (**E**) The cell to the right projects a small membrane ruffle establishing a primordial junction with the neighbouring cell marked by E-cadherin where both GFP-EFA6A and USP9x are co-localized, scale bar 10 μm. (**F**) A newly formed contact along the lateral plasma membrane of two adjacent cells where both GFP-EFA6A and USP9x are co-localized. (**F'**) A magnification of the area outlined in (**F**), scale bar 15 μm. (**G**) The arrowhead points to several cells within a cluster, which upon calcium repletion establish contacts with their surrounding cells in a synchronized manner. Unless otherwise specified all scale bars are 25 μm.

steady state through constitutive ubiquitination and are augmented before TJ formation by deliberate deubiquitination by USP9x. Third, there is a transient translocation of USP9x to primordial cell–cell contacts that accounts for the spatially and temporally regulated increase in EFA6B levels.

With respect to our first finding, previous and current work show that EFA6B is involved in the assembly of a functional TJ in a dose-dependent manner. All together, we make the following observations: (1) in response to the initial cell–cell contact mediated by the E-cadherin, the levels of the endogenous EFA6B increase transiently before the assembly of the TJ; (2) overexpression of EFA6A accelerates the *de novo* assembly of the TJ in a dose-dependent manner (Luton *et al*, 2004) and (3) reduction of the levels of endogenous EFA6B by siRNA delays the assembly of the TJ.

EFA6B possesses high rates of both protein degradation and synthesis that make it an excellent target for effective regulation by the ubiquitin-proteasome system machinery. Exposure to proteasome inhibitors revealed that EFA6B is constitutively poly-ubiquitinated and degraded by the proteasome machinery. Though, at steady state, low levels of EFA6B are maintained as a small pool ready to contribute to the assembly of the TJ in polarizing cells, and to preserve the stability of the TJ in fully polarized cells (Luton *et al*, 2004). During epithelial cell polarization, EFA6B rapidly accumulates at cell–cell contacts before its return to steady-state levels. The drop in EFA6B levels is concomitant with the apparation of poly-ubiquitinated forms of EFA6B. As EFA6B is constitutively ubiquitinated at steady state, one explanation for EFA6B transient accumulation is its protection from proteosomal degradation by a DUB activity. USP9x seemed a logical initial candidate, as it is known to associate with other molecules involved in cell–cell contacts such as afadin, β-catenin and E-cadherin (Taya *et al*, 1998, 1999; Murray *et al*, 2004; Millard and Wood, 2006). Here, we report that in MDCK cells, endogenous EFA6B associates with USP9x uniquely within the first hour after calcium repletion, and importantly, by immunolocalization both proteins were found to co-localize only at nascent cell–cell contacts. Furthermore, their association was coincident with the increase in EFA6B total levels, which could be measured quantitatively by immunoblot and visualized locally at cell–cell contacts by immunofluorescence videomicroscopy. Finally, the association of EFA6B and USP9x, as well as EFA6B accumulation preceded the formation of the TJ, which is thus consistent with their involvement in TJ formation.

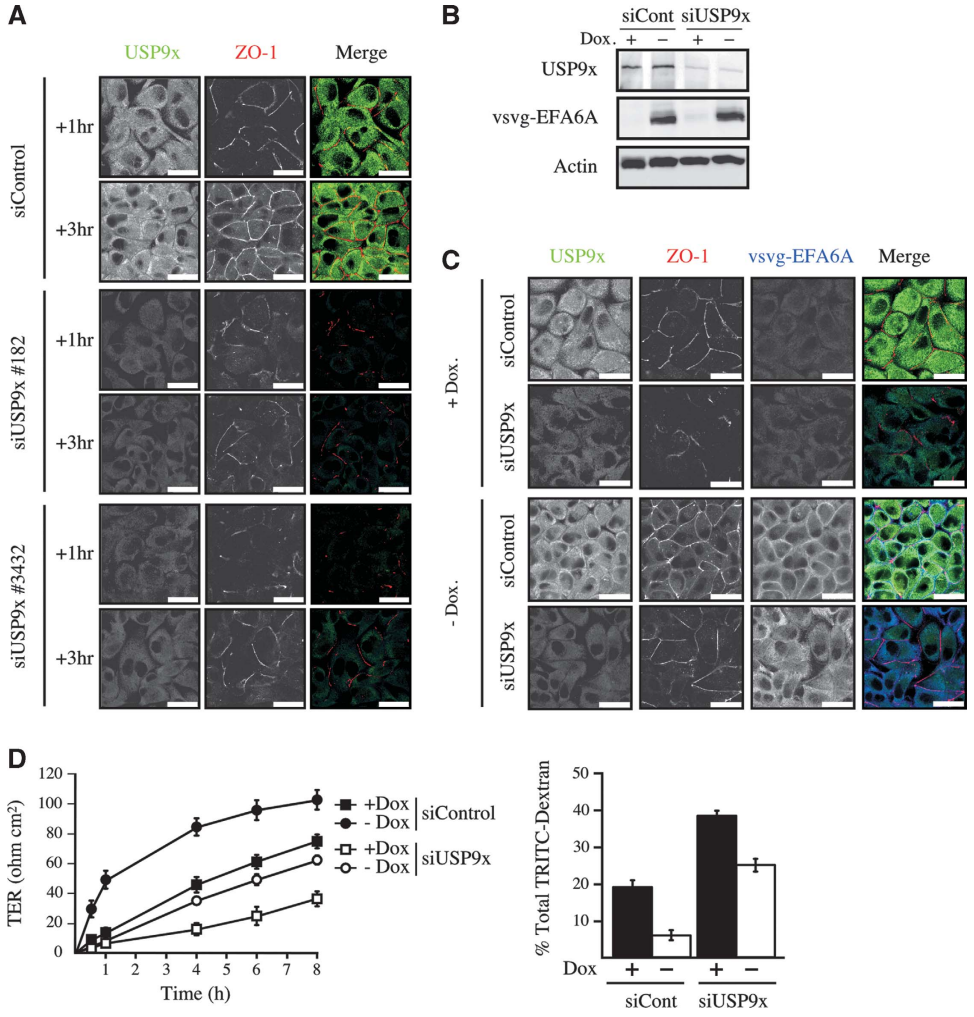


**Figure 6** USP9x promotes TJ assembly via its activity on EFA6. (**A**) MDCK cells were transfected with a control siRNA or two distinct siRNA specific for USP9x (#182 and #3432). At 24 h post-transfection, the cells were subjected to a calcium switch and fixed 1 or 3 h after calcium repletion. The samples were co-stained for USP9x (green) and ZO-1 (red). Scale bars, 25 μm. (**B**) Immunoblots showing USP9x, vsvg-EFA6A and actin levels in tet-off regulated vsvg-EFA6A MDCK cells grown in the absence or presence of doxycyclin (Dox) and transfected with control or USP9x-specific siRNA #182. (**C**) These cells were analysed for their capacity to form functional TJ. Vsvg-EFA6A MDCK cells transfected with control or USP9x (#182) siRNAs and grown in the absence or presence of doxycycline (+/−Dox) were subjected to a calcium switch and fixed 90 min after calcium repletion and processed for IF analysis. The expression and localization of USP9x (green), ZO-1 (red) and vsvg-EFA6A (blue) were examined. Scale bars, 25 μm. (**D**) The gain of TJ barrier function was analysed in a calcium switch assay by measuring the TER over time and the paracellular diffusion of TRITC-dextran at 4 h after calcium repletion +/− siUSP9x #182. For TER measurement $n=5$ and error bars represent the s.e.m. For siControl cells +/−Dox $P<0.0025$ at all times, for siUSP9x cells +/−Dox $P<0.0007$ after 4 h, for +Dox cells +/−siUSP9x $P<0.0014$ after 4 h, for −Dox cells +/− siUSP9x $P<0.0012$ at all times. For the paracellular diffusion of the TRITC-dextran $n=3$ and error bars represent s.e.m. For siControl cells +/−Dox $P=0.0058$, for siUSP9x cells +/−Dox $P=0.0049$, for +Dox cells +/−siUSP9x $P=0.0014$, for −Dox cells +/− siUSP9x $P=0.0012$.

After finding that USP9x was associated with EFA6B, we set out to determine whether USP9x could in fact alter the protein levels of EFA6B, and thus influence the formation of the TJ. Although USP9x knockdown had no effect on steady-state levels of EFA6B in either non-polarized or fully polarized cells, it had a significant effect in cells undergoing the calcium switch assay. USP9x knockdown was found to prevent the accumulation of EFA6B and the subsequent apparition of poly-ubiquitinated forms confirming that the regulation of EFA6B by USP9x is linked to a specific developmental sequence within the epithelial cell. Consistent with its effects on EFA6B, USP9x knockdown delayed the assembly of the TJ, which could then be partially restored by the exogenous expression of EFA6A. Among other proposed substrates of USP9x, there was no effect on the levels of β-catenin nor E-cadherin upon USP9x depletion. In contrast, the expression of afadin was dependent on USP9x regardless of the polarization status of the cells, indicating that deubiquitination of afadin by USP9x is constitutive. Afadin knockdown was shown to delay TJ formation (Sato *et al*, 2006), thus it appears that part of the effect on the TJ formation from USP9x knockdown is through its action on afadin expression. However, exogenous expression of EFA6A was able to partially rescue TJ formation in USP9x-knockdown cells, whereas, exogenous expression of afadin had no effect on TJ formation, and no additional effect when co-expressed together with EFA6A. Thus, we believe that EFA6 is downstream of afadin, and that its effects are independent on the levels of afadin. Note, that EFA6A overexpression or EFA6B repression did not have any effect on afadin levels (data not shown). We conclude that USP9x regulates the TJ assembly in MDCK cells by augmenting the levels of EFA6B as part of

the cascade set in motion by E-cadherin engagement, and at least in part, by maintaining the levels of afadin. In a recent report, Wood and colleagues found that exogenous expression of USP9x in embryonic stem cell-derived neural progenitors resulted in a highly polarized phenotype with respect to the adherens junctional proteins and apical markers (Jolly *et al*, 2009). Taken together, these results suggest a general function for USP9x in the formation of cell–cell junctions during the process of cell polarization.

Our results are consistent with a model whereby the temporal surge in EFA6B levels is generated by the spatiotemporal co-localization of EFA6B with USP9x. We suggest that upon cell–cell contact, both proteins are recruited to and accumulate at the primordial contact zone defined by E-cadherin. In support, we find that the spatial co-localization is coincidental with the timing of EFA6B accumulation, and that EFA6B accumulation is due to USP9x. Analyses by immunofluorescence indicate that the levels of GFP-EFA6A at the contact zone decrease $\sim$30 min after USP9x have already left. We propose that the association of EFA6B to the actin cytoskeleton at the maturing contact zone makes it inaccessible to ubiquitination. A similar mechanism has been proposed to account for the stabilization of β-catenin at the AJ (Murray *et al*, 2004). We do not think that EFA6B is poly-ubiquitinated yet escaping degradation, as we have observed that once EFA6B is poly-ubiquitinated, it is followed by rapid degradation.

In conclusion, epithelial cell polarization has been depicted as the hierarchical assembly of junctional protein modules (Nectin-afadin, E-cadherin-catenin(s), Claudin-ZO) coordinated by the polarity complexes and accompanied by the remodelling of the cortical actin cytoskeleton (EFA6, Par3, Rho-family small GTPases, Arp2/3, WASP, etc) to ultimately orient the cell along its apico-basal axis. An important question is how this cascade of molecular events is orchestrated and regulated in a spatiotemporal manner during epithelium development. Here, we describe a novel signalling pathway that provides a unique regulatory mechanism for the finely tuned spatiotemporal assembly of the TJ. Additional studies are needed to understand how these different pathways are coordinated within the program of cell polarity development.

## Materials and methods

### *Cells*

Madin-Darby canine kidney clone II (MDCK II) and BHK cells were grown, respectively, in MEM (Sigma-Aldrich, France) and GMEM (Invitrogen, France) supplemented with 5% heat decomplemented fetal calf serum (Biowest-Abcys, France) and penicillin-streptomycin (Invitrogen). MDCK cells expressing vsvg-EFA6A under the control of the tetracycline-repressible transactivator have been described elsewhere (Luton *et al*, 2004). The plasmids encoding for GFP-EFA6A full-length and GFP-PH domain of EFA6A were transfected in MDCK cells using the nucleofection AMAXA system (Lonza Group Ltd, Switzerland). After 1 week of selection with geneticin, the cell populations were cell sorted to keep the 10% highest GFP intensity. The MDCK GFP-EFA6A, GFP-PH #1 and GFP-PH #2 geneticin-resistant cell lines used in the experiments were non-clonal populations. MDCK cells were passaged in 10 cm dishes and induced to polarize on 12-mm, 0.4-μm pore size Transwell polycarbonate filters (Corning-Costar, Cambridge, MA) unless otherwise mentioned. The expression of vsvg-EFA6A protein was allowed by growing the cells in the absence of doxycycline (Dox) for 24–36 h before analysis. Transient transfections in MDCK and BHK cells were performed using the nucleofection AMAXA system (Lonza Group Ltd) and the reagent Dreamfect according to the manufacturer's instructions (OZ Biosciences, Marseille, France), respectively.

### *Calcium switch procedure*

On day 1, MDCK cells were plated on 12-mm filters in normal medium, except for the co-immunoprecipitation experiment where 24-mm filters were used. The next day, the cells were subjected to a calcium switch procedure described in detail elsewhere (Luton, 2005). Briefly, the cells were washed three times quickly in PBS-EGTA 2 mM and then three times 10 min under agitation in calcium-free spinner medium (Sigma-Aldrich). The cells were further incubated 6 h in spinner medium supplemented with 5 μM calcium to completely breakdown the TJ as controlled by measuring the TER. At $t=0$, the calcium switch was performed by repletion of calcium using normal medium containing 2 mM calcium. At the indicated times after calcium repletion, the cells were processed for confocal immunofluorescence, biochemical analysis or TJ functional assays as described below.

### *DNA constructs and siRNAs*

The following constructs have been described elsewhere: GFP-EFA6A (Decressac *et al*, 2004), GST-EFA6A, GST-Cter, GST-PHCter, GST-Sec7 (Macia *et al*, 2008), his-EFA6 (Macia *et al*, 2008), GST-S5a and his-myc-ubiquitin (Fallon *et al*, 2006), GST-UIM1 + 2 (ubiquitin-interacting motif 1 and 2) of Eps15 (Regan-Klapisz *et al*, 2005). The PH domain of EFA6A was cloned into pEGFP-C3 (Derrien *et al*, 2002). The mammalian expression vector canine E-cadherin-RFP was a generous gift from Dr James W Nelson (Stanford University, CA) (Perez *et al*, 2008). The cDNAs encoding wild-type USP9x and the catalytic mutant USP9x C1566S were cloned into the mammalian expression vectors pEF6-DEST51 (Invitrogen) containing a V5 and 6xhistidine N-terminal tag (Murray *et al*, 2004). The canine-specific siRNAs were designed and obtained from Eurogentec (Belgium) and named according to the position in the canine cDNA sequence of the first base of the oligonucleotide. For canine EFA6B, the siRNAs were #637 GAGAGUGUGUUCUUUGACAAUCC, #1564 GGCACUUGCUUGACUUCUA, #1770 UGACUUCAGUAGGGCUGUG, for canine USP9x the siRNAs were #182 AAGAUGAGGAACCUG CAUUUC, #3432 AAGGGGUGCUUACCUCAAUGC for canine USP7 the siRNA was #1118 CAGAGAAAGGUGUGAAAUU. The siRNA mismatch of siRNA#637 was CCUAACAGUUUCUUGUGUGAGAG. The control siRNA was the Eurogentec negative control. The analysis of the specificity of the siRNAs is shown in Supplementary Figure S1A for EFA6B and Supplementary Figure S2I for USP9x.

### *Antibodies and reagents*

The following primary antibodies used against the indicated antigen were: rat monoclonal anti-ZO-1 (clone R40.76; Chemicon, UK), rabbit polyclonal anti-claudin 1 (Invitrogen), rabbit polyclonal anti-occludin (Invitrogen), mouse monoclonal anti-E-cadherin (clone 3G8, a gift of Dr W Gallin, University of Alberta, Canada), mouse monoclonal anti-β-catenin (clone 15B8; Sigma-Aldrich), mouse monoclonal anti-afadin (clone 35; BD Biosciences, Belgium), rabbit polyclonal anti-USP7 (Santa Cruz Biotechnology, CA), mouse monoclonal anti-USP9x (Abcam, UK), mouse monoclonal anti-ubiquitin P4G7 (Covance, CA), mouse monoclonal anti-poly-ubiquitin FK1 (BIOMOL International LP, UK), mouse monoclonal anti-actin (clone AC40; Sigma-Aldrich), mouse monoclonal anti-synaptophysin (clone SVP-38; Sigma-Aldrich), rabbit polyclonal anti-GST (GE Healthcare, Belgium), mouse monoclonal anti-6xhistidine tag (clone HIS-1; Sigma-Aldrich), mouse monoclonal anti-V5 tag (Sigma-Aldrich), mouse monoclonal anti-FLAG M2 (Sigma-Aldrich), mouse monoclonal anti-vsvg tag (clone P5D4; Sigma-Aldrich), monoclonal anti-myc tag (murine hybridoma 9E10 and rat hybridoma 3F10; Roche Diagnostics). The rabbit polyclonal anti-USP9x directed against the amino-acids 1–19 of the murine USP9x was described elsewhere (Kanai-Azuma *et al*, 2000). The mouse monoclonal anti-Arf6 (clone 8A6-2) was generated and characterized as described (Marshansky *et al*, 1997). The rabbit polyclonal anti-EFA6B was raised against the Sec7 domain as described elsewhere (Luton *et al*, 2004). Further characterization of the 66 kDa EFA6B isoform is shown in Supplementary Figure S1A–C. Secondary antibodies and phalloidin were from Jackson ImmunoResearch Labs Inc (West Grove, PA). MG-132 and sodium butyrate were from Calbiochem (Merck Chemicals Ltd, UK). All other reagents and chemicals were from Sigma-Aldrich.

#### *Recombinant proteins and pull-down assay*

All GST-EFA6A constructs were in pGEX 3X, his-EFA6A was in pET8c, all GST-USP9x constructs were in pDEST15, GST-UIM1/2-Eps15 in pGEX 5X, GST-S5a in pDEST15. The induction and purification of GST constructs using glutathione-sepharose CL-4B beads (GE Healthcare) was as described earlier (Macia *et al*, 2008). The N-terminal hexahistidine his-EFA6A was purified on Ni-NTA columns according to the manufacturer's instructions (Qiagen, France). For the GST-EFA6A pull-down experiments, MDCK cells were lysed at 4°C in 0.5% Nonidet P-40, 20 mM Hepes pH 7.4, 125 mM NaCl, 1 mM phenylmethylsulphonyl fluoride (PMSF) and a cocktail of protease inhibitors (Complete, Roche Diagnostics). The cleared lysates containing USP9x were incubated 4 h at 4°C with 1.5 μM of the indicated GST-fused proteins and 30 μl of glutathione-sepharose CL-4B beads. After three washes in lysis buffer, the beads were boiled in Laemmli buffer, submitted to SDS–PAGE and USP9x revealed by immunoblot. For the GST-USP9x pull-down experiments, 10 μM of the GST-USP9x fusion proteins and 10 μM of His-EFA6A were incubated together for 2 h at 4°C and the experiments carried on as described above. An aliquot of the mixture was analysed by SDS–PAGE followed by immunoblotting to estimate the total amount of GST-fused proteins, USP9x and his-EFA6 present in the reaction.

#### *Lysates and immunoprecipitation*

Cells were solubilized in SDS lysis buffer (0.5% SDS, 150 mM NaCl, 5 mM EDTA, 20 mM Triethanolamine–HCl pH 8.1, 1 mM PMSF), boiled 10 min, vigorously shaken for 20 min and centrifuged 20 min at 16 000 *g* at room temperature. For cell lysates analysis, the supernatants were transferred into new tubes containing 5 × Laemmli buffer and further boiled 5 min before SDS–PAGE. For immunoprecipitation, the supernatants were transferred into a new tube containing 0.5 ml of ice-cold Triton dilution buffer (5% Triton X-100, 100 mM NaCl, 5 mM EDTA, 50 mM Triethanolamine–HCl pH 8.1, 30 mM *N*-ethylmaleimide (NEM) and the cocktail of protease inhibitors). The samples were then pre-cleared at 4°C for 10 min, centrifuged 10 min 16 000 *g* and combined with protein A-sepharose and the indicated antibody overnight at 4°C. The beads were then washed three times in washing buffer (1% Triton X-100, 0.2% SDS, 150 mM NaCl, 5 mM EDTA, 8% sucrose, NEM 10 mM, 1 mM PMSF and the cocktail of protease inhibitors) and washed once in washing buffer without Triton X-100. The immunoprecipitates were then resuspended and boiled for 5 min in Laemmli buffer before SDS–PAGE and immunoblot analysis. For co-immunoprecipitation of USP9x and EFA6B, MDCK cells grown on 24-mm filters (six filters per immunoprecipitation) were subjected to a calcium switch and lysed in NP-40 lysis buffer (1% NP-40, 125 mM NaCl, 20 mM Hepes pH 7.4, 2 mM PMSF and the cocktail of protease inhibitors) containing the cross-linker DTSP (1 mM) 45 min after calcium repletion. Following overnight immunoprecipitation, the beads were washed four times in lysis buffer without cross-linker and boiled in Laemmli buffer.

#### *Immunoblot*

Samples were resolved on SDS–PAGE and proteins transferred onto a nitrocellulose membrane. Membrane blocking and antibody dilutions were done in PBS 5% non-fat dry milk. For anti-ubiquitin western blot, the proteins were electroblotted onto a PVDF membrane. After transfer, the membrane was denaturated in 6 M guanidine–HCl, 20 mM Tris–HCl pH 7.5, 2 mM DTT, 1 mM PMSF for 30 min at 4°C. The membrane was washed extensively in PBS-Tween 0.1%, blocked in PBS-BSA 5% at room temperature for 6 h and then incubated overnight at 4°C with the indicated antibody diluted in blocking solution. The proteins were revealed by chemiluminescence (ECL™, Amersham France) using secondary antibodies directly coupled to HRP. The membranes were analysed with the luminescent image analyzer LAS-3000 (Fujifilm, France).

#### *Paracellular transport assay and transepithelial electrical resistance (TER) measurement*

The formation of the TJ barrier was assessed during the calcium switch procedure. At the indicated times after calcium repletion, tetramethylrhodamine isothiocyanate (TRITC)-dextran 9 kDa (1 mg/ml in MEM) was added in the apical chamber (200 μl) and 800 μl of MEM was added in the bottom chamber. After 2 h, the total amount of TRITC-dextran in the basal medium was quantitated using a spectrofluorimeter. The graphs report the percentage recovered in the basal medium of the total amount of reagent added apically. All experiments were repeated at least three times using triplicates. The TER was measured as described earlier using triplicates for each measurement (Luton, 2005). Results from at least three independent experiments are expressed in ohms per square centimeter after subtraction of the TER obtained from a duplicate of empty filters.

#### *Confocal immunofluorescence*

When indicated cells were fixed in 4% paraformaldehyde on ice for 30 min rapidly rinsed in PBS-CM (1 mM calcium, 0.5 mM magnesium). The samples were then prepared as described earlier (Luton *et al*, 2004). Images were processed for presentation using NIH Image and Adobe® Photoshop® CS2 software. Images from the calcium switch experiments are representative of at least three independent experiments.

#### *Time-lapse imaging*

The procedure followed has been described in detail elsewhere (Adams *et al*, 1998). Briefly, on day 1, subconfluent MDCK cells grown in a 10-cm Petri dish were passaged 1/10. On day 2, the cells were transfected with the indicated plasmids by nucleofection (AMAXA) according to the manufacturer's instructions and grown overnight in the presence of 5 mM sodium butyrate. On day 3, the cells were trypsinized, washed and plated at low density ($5 \times 10^5$ cells/well of a six-well dish) on collagen-coated coverslips. After 3–5 h, the coverslips were mounted on a pre-warmed motorized stage and analysed on a Leica Sp5 confocal microscope using a × 63 objective. The motorized stage allowed for the acquisition of multiple specimens on the same coverslip. Images were collected at single sites every 1–3 min for 1–3 h at 37°C and 5% $CO_2$. The images were processed as described for confocal immunofluorescence. The movies shown are representative of at least 30 movies of five independent experiments for each condition.

#### *Supplementary data*

Supplementary data are available at *The EMBO Journal* Online (http://www.embojournal.org).

## Acknowledgements

We thank E Lemichez for valuable advice and KL Singer for critical reading of the paper. This work was supported by the Cancéropôle Provence Alpes Cote d'Azur Axe III and the Association pour la Recherche sur le Cancer. DT was the recipient of a post-doctoral fellowship from the Centre National de la Recherche Scientifique.

## Conflict of interest

The authors declare that they have no conflict of interest.

## References

Adams CL, Chen YT, Smith SJ, Nelson WJ (1998) Mechanisms of epithelial cell-cell adhesion and cell compaction revealed by high-resolution tracking of E-cadherin-green fluorescent protein. *J Cell Biol* **142:** 1105–1119

Decressac S, Franco M, Bendahhou S, Warth R, Knauer S, Barhanin J, Lazdunski M, Lesage F (2004) ARF6-dependent interaction of the TWIK1 K+ channel with EFA6, a GDP/GTP exchange factor for ARF6. *EMBO Rep* **5:** 1171–1175

 

Derrien V, Couillault C, Franco M, Martineau S, Montcourrier P, Houlgatte R, Chavrier P (2002) A conserved C-terminal domain of EFA6-family ARF6-guanine nucleotide exchange factors induces lengthening of microvilli-like membrane protrusions. *J Cell Sci* **115:** 2867–2879

Drubin DG, Nelson WJ (1996) Origins of cell polarity. *Cell* **84:** 335–344

Fallon L, Belanger CM, Corera AT, Kontogiannea M, Regan-Klapisz E, Moreau F, Voortman J, Haber M, Rouleau G, Thorarinsdottir T, Brice A, van Bergen En Henegouwen PM, Fon EA (2006) A regulated interaction with the UIM protein Eps15 implicates parkin in EGF receptor trafficking and PI(3)K-Akt signalling. *Nat Cell Biol* **8:** 834–842

Franco M, Peters PJ, Boretto J, van Donselaar E, Neri A, D'Souza-Schorey C, Chavrier P (1999) EFA6, a sec7 domain-containing exchange factor for ARF6, coordinates membrane recycling and actin cytoskeleton organization. *EMBO J* **18:** 1480–1491

Goldstein B, Macara IG (2007) The PAR proteins: fundamental players in animal cell polarization. *Dev Cell* **13:** 609–622

Hershko A, Ciechanover A (1998) The ubiquitin system. *Annu Rev Biochem* **67:** 425–479

Jolly LA, Taylor V, Wood SA (2009) USP9X enhances the polarity and self-renewal of embryonic stem cell-derived neural progenitors. *Mol Biol Cell* **20:** 2015–2029

Kanai-Azuma M, Mattick JS, Kaibuchi K, Wood SA (2000) Co-localization of FAM and AF-6, the mammalian homologues of Drosophila faf and canoe, in mouse eye development. *Mech Dev* **91:** 383–386

Klein S, Partisani M, Franco M, Luton F (2008) EFA6 facilitates the assembly of the tight junction by coordinating an Arf6-dependent and -independent pathway. *J Biol Chem* **283:** 30129–30138

Luton F (2005) The role of EFA6, exchange factor for Arf6, for tight junction assembly, functions, and interaction with the actin cytoskeleton. *Methods Enzymol* **404:** 332–345

Luton F, Klein S, Chauvin JP, Le Bivic A, Bourgoin S, Franco M, Chardin P (2004) EFA6, exchange factor for ARF6, regulates the actin cytoskeleton and associated tight junction in response to E-cadherin engagement. *Mol Biol Cell* **15:** 1134–1145

Macia E, Partisani M, Favard C, Mortier E, Zimmermann P, Carlier MF, Gounon P, Luton F, Franco M (2008) The pleckstrin homology domain of the Arf6-specific exchange factor EFA6 localizes to the plasma membrane by interacting with phosphatidylinositol 4,5-bisphosphate and F-actin. *J Biol Chem* **283:** 19836–19844

Marshansky V, Bourgoin S, Londoño I, Bendayan M, Vinay P (1997) Identification of ADP-ribosylation factor-6 in brush-border membrane and early endosomes of human kidney proximal tubules. *Electrophoresis* **18:** 538–547

Matsuya S, Sakagami H, Tohgo A, Owada Y, Shin HW, Takeshima H, Nakayama K, Kokubun S, Kondo H (2005) Cellular and subcellular localization of EFA6C, a third member of the EFA6 family, in adult mouse Purkinje cells. *J Neurochem* **93:** 674–685

Millard SM, Wood SA (2006) Riding the DUBway: regulation of protein trafficking by deubiquitylating enzymes. *J Cell Biol* **173:** 463–468

Miyoshi J, Takai Y (2005) Molecular perspective on tight-junction assembly and epithelial polarity. *Adv Drug Deliv Rev* **57:** 815–855

Murray RZ, Jolly LA, Wood SA (2004) The FAM deubiquitylating enzyme localizes to multiple points of protein trafficking in epithelia, where it associates with E-cadherin and beta-catenin. *Mol Biol Cell* **15:** 1591–1599

Perez TD, Tamada M, Sheetz MP, Nelson WJ (2008) Immediate-early signaling induced by E-cadherin engagement and adhesion. *J Biol Chem* **283:** 5014–5022

Regan-Klapisz E, Sorokina I, Voortman J, de Keizer P, Roovers RC, Verheesen P, Urbe S, Fallon L, Fon EA, Verkleij A, Benmerah A, van Bergen en Henegouwen PM (2005) Ubiquilin recruits Eps15 into ubiquitin-rich cytoplasmic aggregates via a UIM-UBL interaction. *J Cell Sci* **118:** 4437–4450

Sakagami H (2008) The EFA6 family: guanine nucleotide exchange factors for ADP ribosylation factor 6 at neuronal synapses. *Tohoku J Exp Med* **214:** 191–198

Sakagami H, Suzuki H, Kamata A, Owada Y, Fukunaga K, Mayanagi H, Kondo H (2006) Distinct spatiotemporal expression of EFA6D, a guanine nucleotide exchange factor for ARF6, among the EFA6 family in mouse brain. *Brain Res* **1093:** 1–11

Sakakibara A, Furuse M, Saitou M, Ando-Akatsuka Y, Tsukita S (1997) Possible involvement of phosphorylation of occludin in tight junction formation. *J Cell Biol* **137:** 1393–1401

Sato T, Fujita N, Yamada A, Ooshio T, Okamoto R, Irie K, Takai Y (2006) Regulation of the assembly and adhesion activity of E-cadherin by nectin and afadin for the formation of adherens junctions in Madin-Darby canine kidney cells. *J Biol Chem* **281:** 5288–5299

Shin K, Fogg VC, Margolis B (2006) Tight junctions and cell polarity. *Annu Rev Cell Dev Biol* **22:** 207–235

Sironi C, Teesalu T, Muggia A, Fontana G, Marino F, Savaresi S, Talarico D (2009) EFA6A encodes two isoforms with distinct biological activities in neuronal cells. *J Cell Sci* **122:** 2108–2118

Taya S, Yamamoto T, Kanai-Azuma M, Wood SA, Kaibuchi K (1999) The deubiquitinating enzyme Fam interacts with and stabilizes beta-catenin. *Genes Cells* **4:** 757–767

Taya S, Yamamoto T, Kano K, Kawano Y, Iwamatsu A, Tsuchiya T, Tanaka K, Kanai-Azuma M, Wood SA, Mattick JS, Kaibuchi K (1998) The Ras target AF-6 is a substrate of the fam deubiquitinating enzyme. *J Cell Biol* **142:** 1053–1062

Tsukita S, Furuse M, Itoh M (2001) Multifunctional strands in tight junctions. *Nat Mol Cell Biol* **2:** 285–293

Tsukita S, Yamazaki Y, Katsuno T, Tamura A (2008) Tight junction-based epithelial microenvironment and cell proliferation. *Oncogene* **27:** 6930–6938

Vasioukhin V, Fuchs E (2001) Actin dynamics and cell-cell adhesion in epithelia. *Curr Opin Cell Biol* **13:** 76–84

Woelk T, Oldrini B, Maspero E, Confalonieri S, Cavallaro E, Di Fiore PP, Polo S (2006) Molecular mechanisms of coupled monoubiquitination. *Nat Cell Biol* **8:** 1246–1254

Wong V (1997) Phosphorylation of occludin correlates with occludin localization and function at the tight junction. *Am J Physiol* **273:** C1859–C1867